Element mapping of trapiche rubies

Dr Karl Schmetzer[1], Professor Zhang Beili[2], Gao Yan[2], Dr Heinz-Jürgen Bernhardt[3] and Professor Henry A. Hänni[4]

1. Marbacher Str. 22b, D-85238 Petershausen, Germany
2. National Gemstone Testing Center, Beijing 100034, P.R. China
3. Institut für Mineralogie, Ruhr-Universität, D-44780, Bochum, Germany
4. SSEF Swiss Gemmological Institute, CH-4001 Basel, Switzerland

ABSTRACT: Chemical zoning in trapiche rubies was examined by X-ray microfluorescence analysis and by electron microprobe analysis. Two-dimensional element maps indicate a chemical variability of Al, Si, Ca, Ti, Cr and Fe within the samples. This chemical variation is mainly due to primary growth zoning as well as due to carbonate and in places silicate inclusions in orientated channels of the host rubies. Secondary iron staining caused by intense weathering of the samples is also observed.

Keywords: electron probe, element map, ruby, trapiche, X-ray microfluorescence

Introduction

Trapiche rubies from south-east Asia with a fixed six-rayed star, similar in effect to trapiche emeralds from Colombia, were recently described by Schmetzer *et al.* (1996a). Information available at present indicates that the trapiche rubies come from Myanmar and Vietnam. They consist of six transparent-to-translucent ruby sectors separated by the yellow- or white-appearing arms of a six-rayed star. In some crystals, the six arms (which, unlike typical asteriated gems, are fixed - that is, they do not move when the stone or light source is moved) intersect at one small point, forming six triangular ruby sectors. In many specimens, however, the arms extend outward from a hexagonal central core, producing six trapezohedral ruby areas. The cores are usually opaque yellow or black, but transparent red central areas are also present occasionally.

In the yellow or white arms of the star and in the boundary zones between the core and the six trapezohedral ruby sectors, a massive concentration of tube-like inclusions is observed. These inclusions are orientated perpendicular to morphologically dominant dipyramidal crystal faces; they contain liquid, two-phase (liquid/gas) and solid fillings identified as magnesium-bearing calcite and dolomite by a combination of electron microprobe analysis and micro-Raman spectroscopy. In black or yellow cores, tube-like structures with identical fillings also run parallel to the *c*-axis, i.e. perpendicular to basal faces of the trapiche rubies.

Because tube-like structures that extend into the gem-quality ruby sectors are almost colourless, and the calcite and dolomite inclusions are iron-free, it was concluded that the yellow colour of the arms and some cores must be due to intense weathering and secondary iron staining of the cavities and tubes. This interpretation was supported by

 ISSN: 1355–4565

Table I. *Chemical zoning of trapiche rubies*

	Sample description	*Zoning in*	*Mg*	*Al*	*Si*	*Ca*	*Ti*	*V*	*Cr*	*Fe*
A	Six-rayed star with sharp yellowish-white arms intersecting at one small point	Triangular ruby sectors							z	
		Yellowish-white arms		—	+	++			–	+
B	Six-rayed star with sharp yellow arms intersecting at one small point	Triangular ruby sectors							z	
		Yellow arms		–		++				++
C	Six-rayed star with sharp yellow arms, black core	Trapezoidal ruby sectors								
		Black core		–	+	+++	+	*	–	++
		Yellow arms		–	+	++	+	*		+++
D	Six-rayed star with yellow arms that widen toward the edge, black core	Trapezoidal ruby sectors								
		Black core		—	+	++	+	*		+++
		Yellow arms		—	+	++	+	*		+++
E	Six-rayed star with zoned, sharp yellowish-white (inner part) to yellow (outer part) arms, black core	Trapezoidal ruby sectors							z	
		Black core		–		++			–	+
		Yellowish-white to yellow arms		–		++				+ or ++ (z)
F	Six-rayed star with thin yellow arms without distinct, continuous boundaries to the host, small red core	Trapezoidal ruby sectors							z	
		Red core							+	
		Yellow arms		–		+				+

– smaller concentration than in the six trigonal or trapezohedral ruby sectors
— much smaller concentration than in the six trigonal or trapezohedral ruby sectors
\+ higher concentration than in the six trigonal or trapezohedral ruby sectors
++ much higher concentration than in the six trigonal or trapezohedral ruby sectors
+++ very much higher concentration than in the six trigonal or trapezohedral ruby sectors
z zoning from centre to rim
* not observable in small concentrations due to an overlap of VK_{α} with TiK_{β}

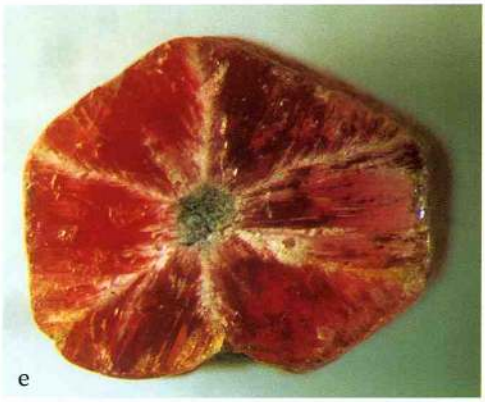

Figure 1a to f: *Hexagonal cross-sections of six trapiche rubies, samples A to F; the arms of the fixed six-rayed stars intersect in a small central point (a,b) or extend outward from the corners of a hexagonal black (c,d,e) or red (f) core. The arms of the stars are yellowish-white (a), yellow (b,c,d,f) or zoned yellowish-white in an inner part and yellow in an outer part of the sample (e). Sizes of the samples are 4.8 mm (a), 3.3 mm (b), 3.2 mm (c), 4.1 mm (d), 4.2 mm (e), and 4.5 mm × 5.0 mm (f).*

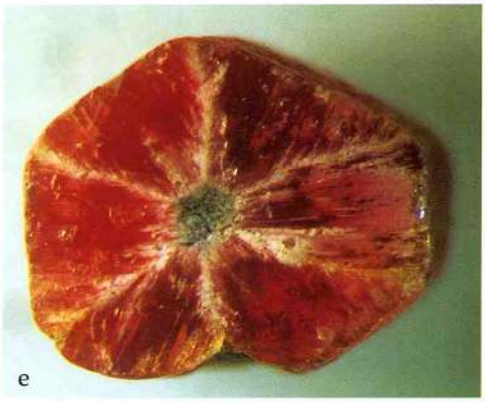

Figure 1a to f: *Hexagonal cross-sections of six trapiche rubies, samples A to F; the arms of the fixed six-rayed stars intersect in a small central point (a,b) or extend outward from the corners of a hexagonal black (c,d,e) or red (f) core. The arms of the stars are yellowish-white (a), yellow (b,c,d,f) or zoned yellowish-white in an inner part and yellow in an outer part of the sample (e). Sizes of the samples are 4.8 mm (a), 3.3 mm (b), 3.2 mm (c), 4.1 mm (d), 4.2 mm (e), and 4.5 mm × 5.0 mm (f).*

X-ray fluorescence analyses of selected trapiche ruby areas with or without a part of a yellow arm.

Two methods were applied to determine the chemical properties of trapiche rubies by Schmetzer *et al.* (1996a) providing analytical data that represent different-size areas within a sample. X-ray fluorescence analysis reveals an average composition of that part of the ruby in an area exposed to the X-ray beam that can be measured in the range of square millimetres. The electron microprobe, on the other hand, is able to analyse much smaller areas with diameters down to about one micrometre.

The chemical variability of a mineralogical sample is, in general, detectable by electron microprobe using two conventional techniques. Preparing X-ray scanning images for selected elements, the intensities of single spots within an image of the area covered by the electron beam are approximately proportional to the concentration of the respective elements. A typical example for trapiche rubies, which was given in the previous paper, showed the distribution of calcium and magnesium in calcite and dolomite as fillings of single orientated tube-like structures and covered an area of approximately 100 x 100 μm (0.1 x 0.1 mm). According to the experimental conditions of the instrument, this technique – which is performed with a fixed, non-moving sample – is limited to the examination of sectors which cover a maximum area of about 200 x 200 μm (0.2 x 0.2 mm).

Another technique for the evaluation of chemical variability of a sample by electron microprobe is performed with a moving stage, i.e. a moving sample and a fixed electron beam, in order to prepare various scans across the surface of the sample. A typical traverse across a ruby crystal or another gemstone to show its chemical variability consists of about 30 to 120 point analyses within a scan length in the mm range (see Peretti *et al.*, 1995; Schmetzer *et al.*, 1996b). Using this particular technique, information about chemical zoning along single traverses across a sample is obtainable.

The application of the two conventional methods described, however, is unable to provide two-dimensional information about element concentrations and chemical variability in minerals, which is of great interest in trapiche rubies.

The present paper describes two different techniques for the determination of two-dimensional element maps in trapiche rubies, which have been only rarely applied to the characterization of gem materials. Using trapiche rubies as an example, the techniques described are able to fill the gap between conventional X-ray fluorescence analysis and conventional electron microprobe techniques.

Materials

For the present study six slices of trapiche rubies were cut in a direction perpendicular to the c-axis of the corundum crystals. The samples were selected in order to cover the variability of structural features in trapiche rubies (see *Table I*). In detail, samples were selected with six-rayed stars intersecting at one small point (*Figure 1a, b*) as well as trapiche rubies with black (*Figure 1c, d, e*) or red (*Figure 1f*) cores. Parts of the samples revealed sharp yellowish-white (*Figure 1a*) or yellow (*Figure 1b, c*) arms, and one sample showed a colour zoning within the six sharp arms of the star with yellowish-white central parts and stronger yellow outer parts (*Figure 1e*). In one sample, the six yellow arms of the star widen toward the rim of the crystal (*Figure 1d*), and in one trapiche ruby, only thin yellow arms without continuous boundaries to the six trapezohedral ruby sectors were observed (*Figure 1f*).

Results

X-ray microfluorescence (XRMF) analysis

Chemical zoning was observed in all six samples of trapiche rubies examined with the OMICRON XRMF system. Different element concentrations were found for Al, Ca and Fe in all samples as well as for Si, Ti and Cr in parts of the samples. No chemical inhomogeneities were proven for Mg and V with the experimental conditions applied (*Table I*).

Methods

Data collection procedures

A well-known technique to display two-dimensional element distributions of sample areas is to scan the electron beam of an electron microprobe (or of a scanning electron microscope) and to collect the signals for image development using a wavelength dispersive spectrometer (WDS), which has been set to the position of the required characteristic X-radiation. Another possibility is to use the signals of a selected range of channels of an energy dispersive spectrometer (EDS) representing the requested radiation. The signals are displayed in real time on a screen which is synchronized with the scanning system of the microprobe. In modern systems, these signals may be stored and accumulated in order to display the complete image. In the latter case the signals of more than one element can be acquired simultaneously. Limiting factors are the number of WDS facilities available on the microprobe or the maximum number of energy regions allowed by the EDS software.

Using WDS systems, the analysed sample, the diffracting crystal and the detector must be on one circle (*Figure 2a*). According to these optical and geometrical conditions, only small areas of a sample can be examined with a fixed sample stage. Because it is not possible to scan an X-ray beam, X-ray fluorescence techniques cannot be used for this kind of imaging procedure.

In order to overcome the problems mentioned, a different kind of image generation can be applied. For these techniques the electron beam or a strongly collimated beam of primary X-rays of a microfluorescence system remains fixed at one position and the sample with its sample stage is moved in two orthogonal directions under the fixed beam covering the sample area of interest. In these

Figure 2a: *Schematic drawing of the experimental conditions in the electron microprobe for element mapping of larger areas showing the incident electron beam, the moving sample stage, the fixed diffracting crystal and the X-ray detector; the diffracting crystal and the detector form a wavelength dispersive spectrometer (WDS).*

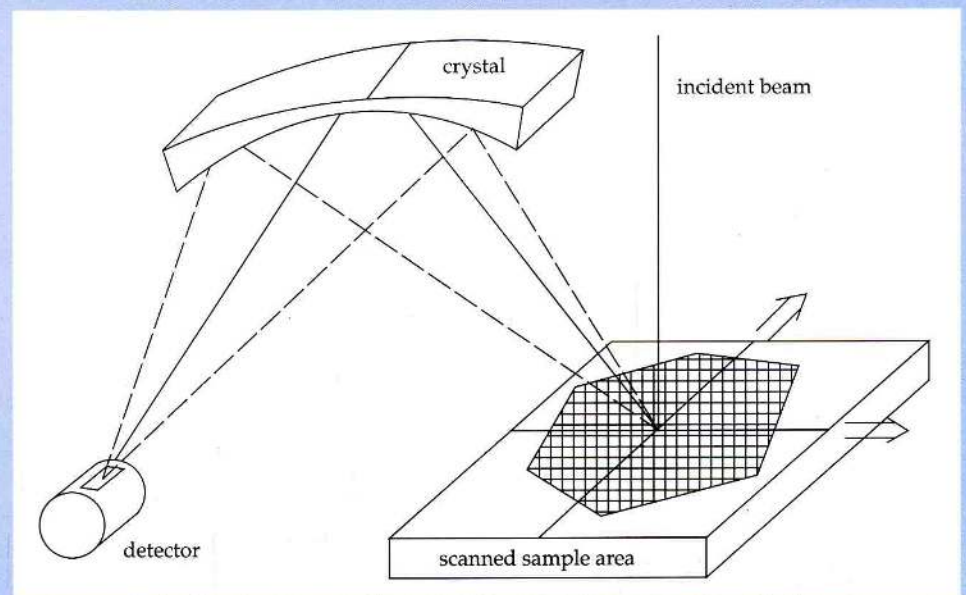

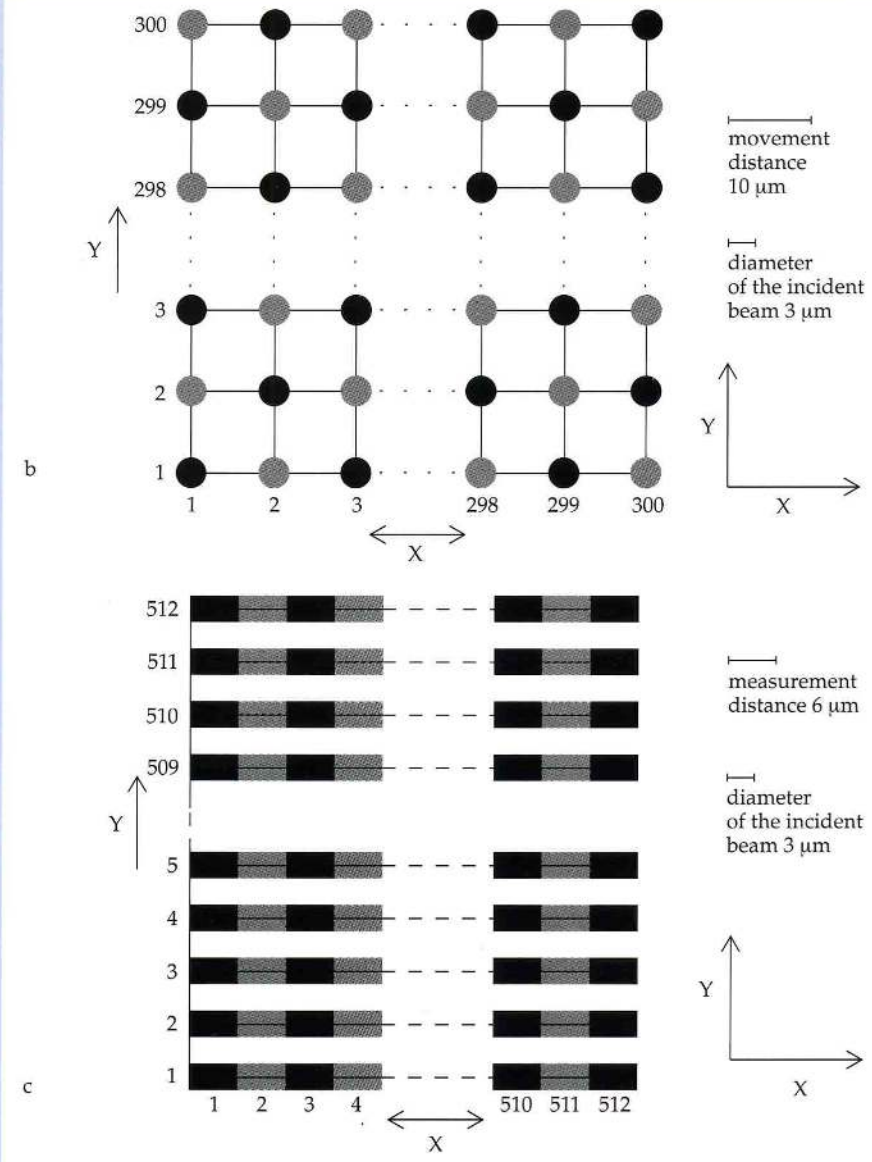

Figure 2b, c: *Data collection for element mapping by XRMF and EMPA in a step-by-step (b) or continuous raster mode (c); the analytical details of Figure 2b represent the data collection for a trapiche ruby by electron microprobe with a step-by-step measuring distance of about 10 µm and a beam diameter of approximately 3 µm; the analytical details of Figure 2c represent data collection for a trapiche ruby by electron microprobe in a continuous raster mode with a beam diameter of approximately 3 µm and a line length of about 6 µm; analysed areas are hatched, arrows indicate the direction of the moving stage. For element mapping by XRMF analysis an X-ray beam with a diameter of 70 µm was used in a continuous raster mode, i.e. overlapping areas within the sample were measured several times.*

systems, in addition to the elements to be analysed and the sample area, the user has also to select the desired resolution, i.e. the number of data points on the analysed sample area which form a regular, rectangular grid on the sample surface. Each point of such a grid represents one pixel in the later X-ray image. Furthermore, the counting time for each measuring point has to be selected. Two slightly different data collection procedures are possible:

(a) In a non-continuous analysis mode (*Figure 2b*) the sample is moved to a point of the rectangular grid and then the counting time is started. The measured intensity signal of the fluorescence radiation represents the element concentration of the currently excited sample volume which mainly depends on the beam diameter. On completion of the selected counting time, the measuring procedure is stopped and the sample is moved to the next point of the grid. This is a step-by-step procedure.

(b) In a continuous analysis mode (*Figure 2c*) along the movement of the sample between two grid points, the intensity of the specified characteristic X-radiation is continuously measured by the detector. The resulting intensities represent the average element concentrations of the excited sample volume between the two points of the rectangular grid. The position of the data point in the pixel-by-pixel image is set to the middle between the two adjacent points of the grid in the direction of movement.

In both modes the counting results of each point for each element are stored. Subsequent to the complete measuring procedure of the selected sample area, using special computer software the intensities of each element are linked to a colour or to a grey scale. Each data point is classified and plotted on a screen according to a corresponding colour with respect to its original position on the sample surface. Thus, an enlarged image of the sample is produced representing the element composition of one element in the sample. The images can be treated mathematically, e.g. intensity relations between two elements may be computed and depicted. The element distribution can be stored and printed depending on the capabilities of the computer programme in use.

Element mapping using X-ray microfluorescence analysis (XRMF)

Element mapping by XRMF was developed in the mid-'eighties by several working groups in Japan and in the United States (Kobayashi *et al.*, 1985; Nichols and Ryon, 1986; Wherry and Cross, 1986). A commercially available analysis system was designed by Kevex Instruments and marketed with the trade name OMICRON. The OMICRON system and similar facilities were applied for element mapping of metals, alloys, rocks and minerals, but also for organic matter, e.g. leaves, tissues and bones (Boehme, 1987; Nichols *et al.*, 1987; Cross and Wherry, 1988; Wherry and Cross, 1988; Carpenter *et al.*, 1989; Carpenter and Taylor, 1991; Kobayashi *et al.*, 1991; Cross *et al.*, 1992; Rindby *et al.*, 1992; Voglis *et al.*, 1993; Carpenter *et al.*, 1995a,b). XRMF was compared by Pozsgai (1991) with similar techniques, e.g. X-ray fluorescence in the electron microscope or X-ray fluorescence excited by synchrotron radiation.

For the preparation of element images of trapiche rubies, a conventional OMICRON system (*Figure 3*) was used. The data collection and handling of this analytical facility was briefly described by Nichols *et al.* (1987) and a schematic drawing of the OMICRON analysis system is given by Cross and Wherry (1988).

In the analytical facility available for the present study, the diameter of the primary X-ray beam could be varied between 50 and 2000 μm. However, the best spatial

Figure 3: The OMICRON XRMF analysis system consisting of the basic measurement unit (right) colour TV sample display (centre) and computer-based data processor (left).

resolution and intensity versus background conditions were obtained in vacuum with a collimator diameter of 70 μm. The examination of the six trapiche ruby samples of about 3 to 5 mm in size was performed in a continuous raster mode (see *Figure 2c*) with 250 analytical data collection steps along both X and Y directions of the sample stage. Consequently, a single X-ray image of one sample contains information from 62 500 single grid points. With a beam diameter of 70 μm, each grid point represents an area of ruby and a possible range of inclusions in that area. The energy dispersive X-ray fluorescence spectra obtained during the continuous movement were collected with a Si (Li) detector. The required measuring time was about two to three hours. As the data collection was repeated up to four times for each ruby sample, the examination of one trapiche ruby was carried out over 8 to 12 hours. The collected data were processed by image-forming software to complex two-dimensional element images consisting of 62 500 pixels each. Element maps were prepared for eight elements, namely Mg, Al, Si, Ca, Ti, V, Cr and Fe (the OMICRON system allows the simultaneous acquisition of up to 25 element maps from one set of analytical data).

Element mapping using electron microprobe analysis (EMPA)

The data acquisition procedure by electron microprobe is similar to that of XRMF. As WDS facilities (see *Figure 2a*) have much better wavelength resolution than EDS systems and better peak-to-background ratios, WDS images are much clearer than EDS images. Thus, data collection by WDS systems is preferred for element mapping by electron microprobe. According to the number of WDS facilities available in the analytical system of a microprobe (up to five spectrometers in modern instruments), the number of elements which can be mapped simultaneously is limited to five. For mapping of additional elements, the run is repeated with new spectrometer settings. From experience it was found that expressive images should consist of at least 30 000 pixels representing single points in the rectangular grid. This corresponds to about 12 hours of acquisition time with, for example, one second counting time for each analytical point (plus processing time, plus time for moving the sample stage if data collection in a non-continuous raster mode is applied). Consequently, this technique is time consuming and requires an extremely stable microprobe system (Bernhardt *et al.*, 1995).

For the evaluation of this technique to gemmological problems element maps were performed for one trapiche ruby (sample C, *Figure 1c*) in both analytical modes mentioned above, i.e. in non-continuous and continuous raster modes.

A first run was done with a CAMECA Camebax electron microprobe for three elements, Al, Ca and Fe. Data were collected step by step along a rectangular grid with point distances of 10 μm during an analysis time of 1 second at each of the 90 000 analysis points (see *Figure 2b*). For this measurement, an analysis time of 35 hours was needed.

A second run was performed with a CAMECA Camebax SX50 electron

microprobe facility for Al, Si, Ca and Fe. Using the four wavelength dispersive spectrometers of the microprobe, data were collected in continuous raster mode along a scan line of approximately 6 µm for 512 lengths along the X and for 512 lengths along the Y direction of the sample (*Figure 2c*). Consequently, the element images consist of 262 144 pixels each. Data collection was performed during a period of 0.2 seconds along each measuring distance of about 6 µm, and approximately 15 hours were needed for the complete measurement procedure for mapping of the four elements mentioned.

For image formation, special data handling and image-forming software written by one of the authors (H.-J.B.) was applied.

Characterization of inclusions

The examination of the six trapiche rubies by X-ray microfluorescence analysis revealed extraordinarily high concentrations of Si, Ti and Fe in the six arms of the samples C and D. For the characterization of inclusions in the orientated channels of these two trapiche rubies (in addition to the previously identified calcite and dolomite fillings), several channels in both samples were analysed by electron microprobe using conventional energy dispersive and wavelength dispersive systems of a CAMECA Camebax SX50 electron microprobe.

The image processing software of the analytical system generates element images of the samples, in which a colour code is used for varying concentrations between different analysis points. Variable element concentrations are displayed pixel by pixel in the X-ray image in the sequence (from low to high concentrations) violet → blue → green → yellow → red and examples of Ca and Fe are shown in *Figure 4a, b*.

Element distribution maps of samples A, B and D are presented in *Figures 5 to 7*. In all samples, we observed a distinctly smaller aluminium concentration in the yellow or yellowish-white arms of the stars as well as in the black cores of samples C, D and E compared to the aluminium concentration of the six triangular or trapezohedral ruby sectors. This was also observed for chromium in the yellowish-white arms of sample A (*Figure 5*) and in the black cores of samples C and E. The red core of sample F, on the other hand, revealed a higher chromium concentration than the six trapezohedral ruby sectors of the sample. In four trapiche rubies, a distinct chromium zoning within the six triangular (samples A and B; *Figure 6*) or the six trapezohedral ruby sectors (samples E and F) was also observed.

Figure 4a, b: *Element maps of Ca (left) and Fe (right) for trapiche ruby, sample C, obtained by XRMF analysis. Different element concentrations are displayed pixel by pixel in the XRMF map; increasing concentrations are colour coded in the sequence violet → blue → green → yellow → red.*

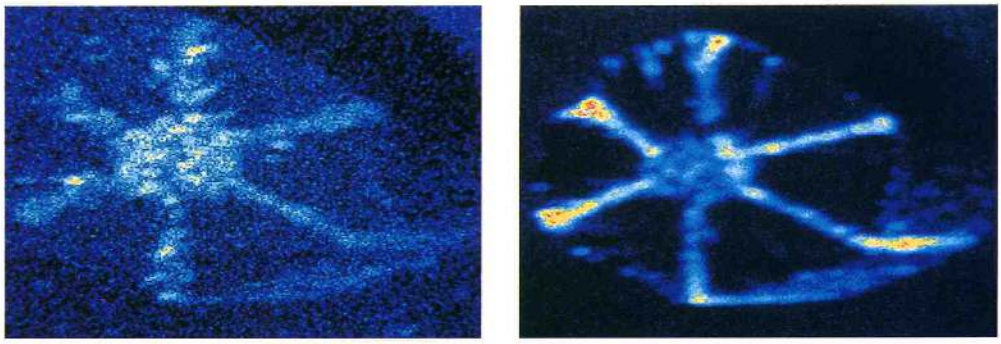

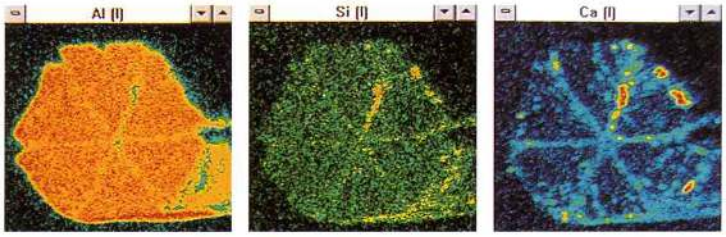

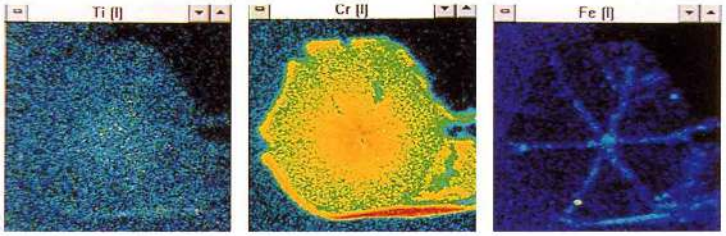

Figure 5: *Element distribution maps for trapiche ruby, sample A, obtained by XRMF analysis; the six yellowish-white arms of the sample intersect at one small central point.*

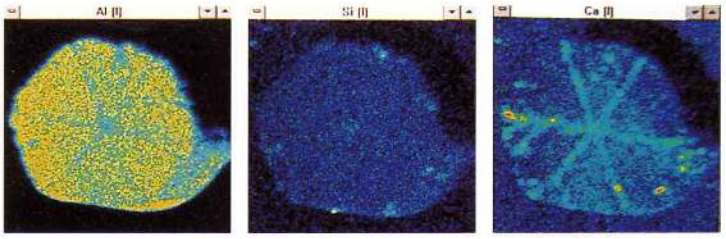

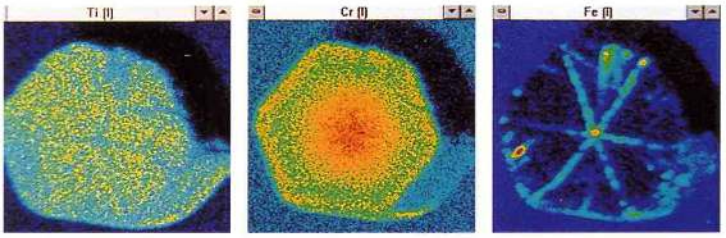

Figure 6: *Element distribution maps for trapiche ruby, sample B, obtained by XRMF analysis; the six yellow arms of the sample intersect at one small central point.*

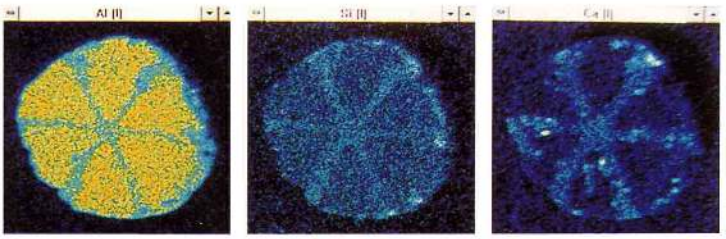

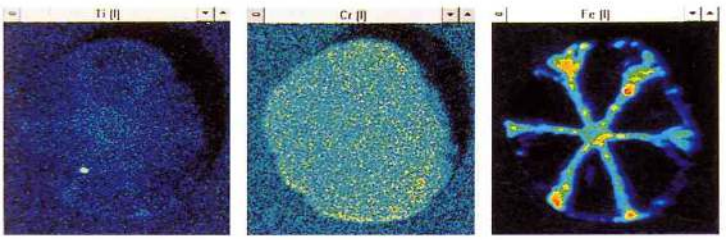

Figure 7: *Element distribution maps for trapiche ruby, sample D, obtained by XRMF analysis; the six broad yellow arms of the sample extend outward from a hexagonal black core.*

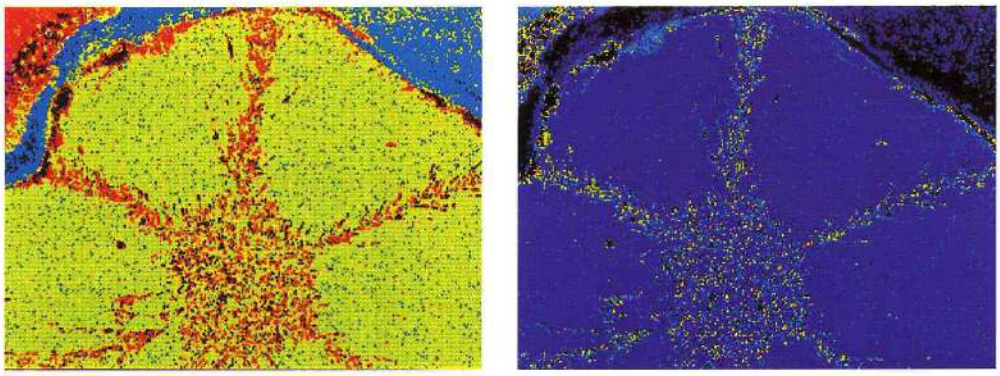

8a

Figure 8: *Element maps of Al, Si, Ca and Fe for trapiche ruby, sample C, obtained by EMPA. Different element concentrations are displayed pixel by pixel in the XRMF map; increasing concentrations are colour coded in the sequence violet → blue → green → yellow → red; (a) two element maps for Ca are given, which were obtained from data collected in a step-by-step measuring mode, different colour codes are applied for image forming according to the counting rates measured at each analysis point; (b) four element maps for Al, Si, Ca and Fe were obtained from a continuous raster mode.*

8b

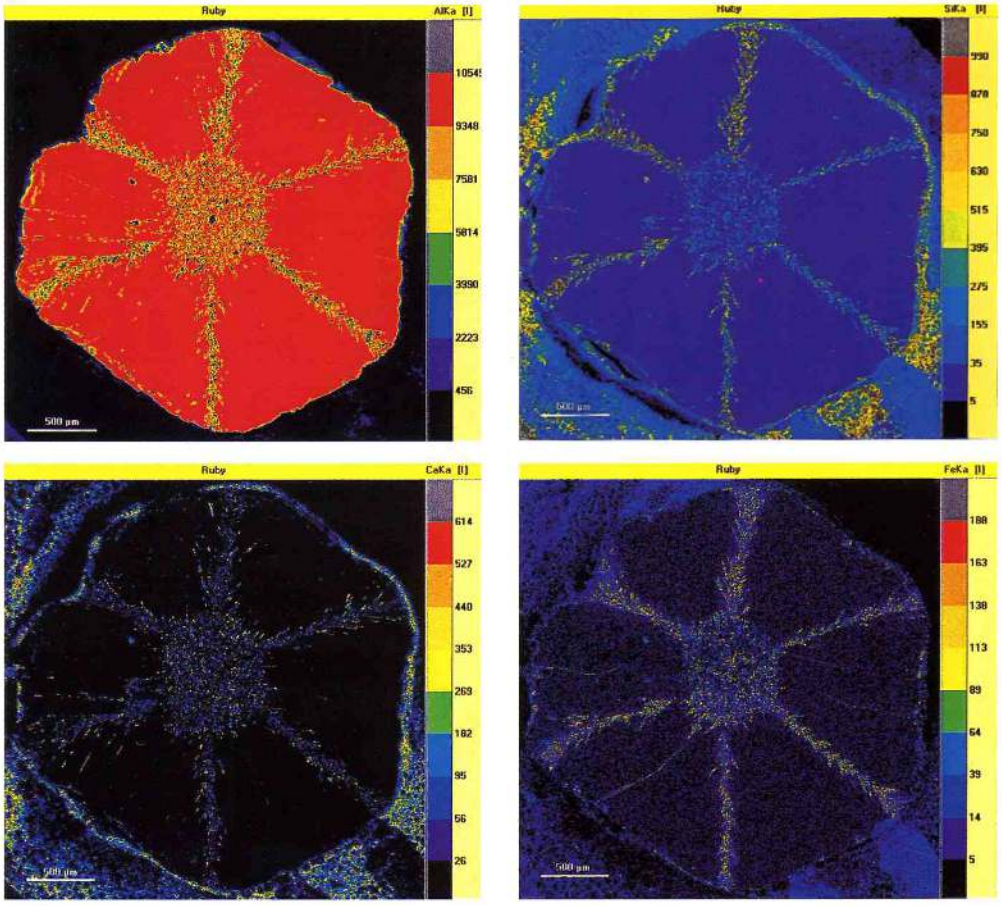

Various calcium concentrations due to inclusions of calcite and dolomite (see Schmetzer *et al.*, 1996a) were found in the yellowish-white or yellow arms of all six samples and in the black cores of samples C, D and E. Any variation of magnesium concentration caused by the dolomite inclusions, on the other hand, was not resolved with the measuring conditions used. This result is consistent with decreasing sensitivity of the instrument towards lighter elements.

Iron was also observed in various concentrations in the arms of the six-rayed stars as well as in black cores. In general, yellowish-white arms (sample A, *Figure 5*) or yellowish-white inner parts of zoned arms (sample E) revealed smaller iron concentrations than the yellow outer parts of zoned arms (sample E) or completely yellow arms (samples B, C and D, *Figures 6 and 7*). No iron was found in the six triangular or trapezohedral ruby sectors of all six samples or in the red core of sample F.

A somewhat unexpected result was the observation of distinct concentrations of silicon in the yellowish-white arms of sample A (*Figure 5*) and of silicon and titanium in the yellow arms and black cores of samples C and D (*Figure 7*).

Electron microprobe analysis (EMPA)

The mapping of Al, Si, Ca and Fe in sample C by electron microprobe (*Figures 8a,b*) confirms the analytical results obtained by XRMF. According to the smaller diameter of the electron beam of the microprobe, a somewhat higher resolution is obtained for these element maps (compare *Figure 1c* and *Figures 4a,b*). In both analysis procedures applied, i.e. in a step-by-step (*Figure 8a*) and in a continuous raster mode (*Figure 8b*), no significant differences between the element images were observed. Iron contents were observed in the core and in the six arms of the star as well as in different small irregular fissures.

Characterization of inclusions

XRMF of trapiche rubies C and D revealed extraordinarily high concentrations of Si, Ti and Fe in the yellow arms and in the black cores of the samples. Semi-quantitative and quantitative chemical examination of several inclusions within these zones were performed by single-point analyses using the energy dispersive and wavelength dispersive analytical systems of the microprobe. These analyses of solid inclusions in orientated channels proved the presence of K–Al- and Fe–Al-silicates with or without titanium contents in addition to the previously identified calcite and dolomite fillings (see also Schmetzer *et al.*, 1996a). Quantitative chemical analyses, however, gave extremely variable results and proved compositions of the silicates in the channels to be inhomogeneous. From these results, it is concluded that the channels contain several extremely fine-grained silicate minerals.

Discussion

Chemical zoning in trapiche rubies has been proved by element mapping using XRMF and EMPA techniques. Three overlapping effects were observed in the samples (*Table I*):

(a) Chromium zoning within trigonal or trapezohedral ruby sectors (samples A, B, E and F) or between a red core and six trapezohedral ruby sectors (sample F) is due to growth zoning which is not related to inclusions in orientated channels.

(b) Calcite, dolomite and K–Al–Fe–Ti-silicate inclusions in the yellowish-white to yellow arms of all samples and in the black cores of samples C, D and E, cause aluminium and chromium deficiencies and variable concentrations of Si, Ca, Ti and Fe in these areas.

(c) A third mechanism contributing to the chemical inhomogeneity of trapiche rubies is caused by iron staining of primary tube-like cavities and secondary irregular fissures due to intense weathering of most samples. A distinct zoning with intensely weathered yellow arms in the outer parts and less weathered yellowish-white arms in the inner part of sample E (*Figure 1e*) is correlated with higher iron contents in the more weathered parts (*Table I*).

In summary, element mapping of trapiche rubies reveals a characteristic primary growth zoning, the presence of carbonate and some silicate mineral inclusions in orientated channels, and secondary weathering and iron-staining of the samples.

Conclusions

Element mapping by XRMF or EMPA is an extremely useful tool to understand various effects of chemical zoning within gem materials. Possible applications of element mapping to gemmological testing problems are the distinction of natural and synthetic gem materials due to variable chemical growth zoning as well as providing proof of diffusion treatments as recently demonstrated by Zhang *et al.* (1997).

Different diameters of incident X-ray or electron beams (70 or 3–4 μm respectively) were applied to excite characteristic X-ray fluorescence radiation in the samples and these give different spatial resolutions.

XRMF facilities include image-producing software packages which are nowadays routinely available (e.g. the OMICRON system by Kevex Instruments). The more time-consuming element mapping by electron microprobe requires extremely stable instrumental conditions and specially developed image-processing software applied to the data collection.

Acknowledgement

The authors are grateful to Dr H. Fiedler of Getac Instrumentebau, Mainz, Germany, for providing information about the OMICRON system.

References

Bernhardt, H.J., Massonne, H.J., Reinecke, T., Reinhardt, J., and Willner, A., 1995. Digital element distribution maps, an aid for petrological investigations. *Beihefte zum European Journal of Mineralogy*, **7**(1), 28

Boehme, D.R., 1987. X-ray microfluorescence of geologic materials. *Advances in X-ray Analysis*, **30**, 39– 44

Carpenter, D.A., Gorin, A., and Shor, J.T., 1995b. Analysis of heterogeneous materials with X-ray microfluorescence and microdiffraction. *Advances in X-ray Analysis*, **38**, 557–62

Carpenter, D.A., and Taylor, M.A., 1991. Fast, high-resolution X-ray microfluorescence imaging. *Advances in X-ray Analysis*, **34**, 217–21

Carpenter, D.A., Taylor, M.A., and Holcombe, C.E., 1989. Applications of a laboratory X-ray microprobe to materials analysis. *Advances in X-ray Analysis*, **32**, 115–20

Carpenter, D.A., Taylor, M.A., and Lawson, R.L., 1995a. High-resolution X-ray microfluorescence imaging with a laboratory-based instrument. *Journal of Trace and Microprobe Techniques*, **13**(2) 141–61

Cross, B.J., Lamb, R.D., Ma, S., and Paque, J.M., 1992. Large-area X-ray microfluorescence imaging of heterogeneous materials. *Advances in X-ray Analysis*, **35**, 1255–64

Cross, B.J., and Wherry, D.C., 1988. X-ray microfluorescence analyser for multilayer metal films. *Thin Solid Films*, **166**, 263–72

Kobayashi, Y., Fukumoto, N., and Kurahashi, M., 1991. X-ray fluorescence element-mapping spectrometer with improved spatial resolution. *Measurement Science and Technology*, **2**, 183–4

Kobayashi, Y., Kawase, A., Uchiumi, A., Nakamura, S., Kubota, M., Nakatani, K., Ban, H., and Arai, T., 1985. Element mapping by X-ray fluorescence spectrometry. *Analytical Sciences*, **1**, 13–17

Nichols, M.C., Boehme, D.R., Ryon, R.W., Wherry, D., Cross, B., and Aden, G., 1987. Parameters affecting X-ray microfluorescence (XRMF) analysis. *Advances in X-ray Analysis*, **30**, 45–51

Nichols, M.C., and Ryon, R.W., 1986. An X-ray microfluorescence analysis system with diffraction capabilities. *Advances in X-ray Analysis*, **29**, 423–6

Peretti, A., Schmetzer, K., Bernhardt, H.-J., and Mouawad, F., 1995. Rubies from Mong Hsu. *Gems & Gemology*, **31**(1), 2–26

Pozsgai, I., 1991. X-ray microfluorescence analysis inside and outside the electron microscope. *X-ray Spectrometry*, **20**(5), 215–23

Rindby, A., Voglis, P., Nilsson, G., and Stocklassa, B., 1992. Software development for X-ray microbeam spectroscopy. *Advances in X-ray Analysis*, **35**, 1247–54

Schmetzer, K., Hänni, H.A., Bernhardt, H.-J., and Schwarz, D., 1996a. Trapiche rubies. *Gems & Gemology*, **32**(4), 242–50

Schmetzer, K., Peretti, A., Medenbach, O., and Bernhardt, H.-J., 1996b. Russian flux-grown synthetic alexandrite. *Gems & Gemology*, **32**(3), 186–202

Voglis, P., Attaelmanan, A., Engström, P., Larsson, S., and Rindby, A., 1993. Element mapping of bone tissues by the use of capillary focused XRF. *X-ray Spectrometry*, **22**, 229–33

Wherry, D., and Cross, B., 1986. XRF, microbeam analysis and digital imaging combined into powerful new technique. *Kevex Analyst*, **12**, 8–9

Wherry, D., and Cross, B.J., 1988. Applications of small-area X-ray fluorescence analysis using a microbeam X-ray source. *Spectroscopy*, **3**(8), 38–40

Zhang, B.L., Gao, Y., and Li, J.Z., 1997. Research on Ti and Cr diffusion treated star sapphires. *26th International Gemmological Conference, Abstract Volume*, 5–6